STRUCTURAL CONTROL AND HEALTH MONITORING
Struct. Control Health Monit. 2008; **15**:90–116
Published online 4 April 2007 in Wiley InterScience
(www.interscience.wiley.com) DOI: 10.1002/stc.208

Impulse response analysis of the Van Nuys 7-storey hotel during 11 earthquakes and earthquake damage detection

Maria I. Todorovska*,†,‡ and Mihailo D. Trifunac§

Department of Civil Engineering, University of Southern California, Los Angeles, CA 90089-2531, U.S.A.

SUMMARY

Wave travel times of vertically propagating waves are measured in the Van Nuys 7-storey hotel, located in the Los Angeles metropolitan area, from impulse response functions computed by deconvolution of the recorded earthquake response. East-West response data from 11 earthquakes over a period of 24 years are analysed. Changes in wave travel times are used to infer about local (between sensors) and global changes of structural stiffness, from one event to another, and with time during the earthquakes that damaged the building (San Fernando and Northridge). Also, wave travel times are used to estimate the fundamental fixed-base frequency of the building, f_1, which is compared with independent estimates of the soil–structure system frequency f_{sys} during the same earthquakes and during five ambient vibration tests. The analysis shows that monitoring only the changes of f_{sys} can be misleading for structural health monitoring and can lead to erroneous alarms, while monitoring changes of f_1 over suitably chosen time windows (before, during, and after excitation by strong earthquake motions) can be a powerful and robust tool for structural health monitoring. It is concluded that, under favourable conditions, this method can be used as a tool for global and local structural health monitoring. Copyright © 2007 John Wiley & Sons, Ltd.

KEY WORDS: earthquake damage detection; structural health monitoring; wave propagation in buildings; impulse response function; deconvolution; Van Nuys hotel

1. INTRODUCTION

Structural health monitoring methods are validated and calibrated best by using response data of full-scale structures to actual events that have damaged the structure. Data from *multiple* events, causing different levels of response, are particularly valuable. Such data are, however, limited, rarely sufficient, and almost never complete to allow unequivocal and unique interpretation. The Van Nuys 7-storey-reinforced concrete (RC) hotel is a rare example of a

*Correspondence to: Maria I. Todorovska, Department of Civil Engineering, University of Southern California, Los Angeles, CA 90089-2531, U.S.A.
†E-mail: mtodorov@usc.edu
‡Research Professor.
§Professor.

Received 14 August 2006
Revised 8 February 2007
Accepted 23 February 2007

building instrumented by a seismic monitoring system, and damaged by earthquakes. There are strong motion records of 12 earthquakes recorded in this building over a period of 24 years (between February 1971 and December 1994). Two of these earthquakes caused visible damage. Five ambient vibration tests of the building have also been conducted, two of which have been comprehensive. Also, supporting information and results of many studies are available for this building [1–17]. The objective of this paper is to use these data to explore further the capabilities of a new structural health monitoring method that is based on detecting changes in wave travel times through the building, measured from impulse response functions computed by deconvolution of recorded seismic response. (A longer version of this study can be found in Reference [18]).

Measuring wave travel times using impulse response functions computed by deconvolution, to the knowledge of the authors, was first applied to buildings by Snieder and Şafak [19], who studied one-dimensional (1D) wave propagation in Millikan Library in Pasadena, California, during small amplitude seismic response. It was also applied to small amplitude response of the Factor building in Los Angeles, California [20]. This method was first applied to earthquake damage detection by Todorovska and Trifunac [21] on the Imperial County Services building—a 6-storey RC structure in El Centro, California, damaged by the Imperial Valley earthquake of 15 October 1979. Their study showed that the results from the impulse response analysis were consistent with results from other structural health monitoring methods [22, 23], and that the method is promising and should be further developed. What is different for the Van Nuys building, studied in this paper, is that it was damaged by *two* earthquakes, both recorded in the building, and that records of other smaller or distant earthquakes are also available. This would provide useful information about the variations of the monitored quantity that are not related to damage, and about the threshold change that is related to damage.

Most health monitoring methods for civil engineering structures use structural vibration data, and are based on detecting changes in their *modal* parameters—frequencies and mode shapes (e.g. see References [24, 25] for detailed state-of-the-art reviews on this topic). While monitoring changes of the frequencies of vibration requires minimum instrumentation, monitoring changes of the mode shapes requires more extensive instrumentation not available in most instrumented structures. Further, the frequencies of vibration are usually estimated using some energy distribution of the recorded response in the time-phase plane.

There are two main advantages of the method used in this paper, which is a *wave* method, over the modal methods. One advantage is that it is *local* (the wave travel times between sensors depend only on the properties of the structure between the sensors), while the modal methods are *global* (the modal properties depend on the overall properties of the structure, hence changing little when the damage is localized). As a consequence, the wave methods can detect local changes with relatively few sensors (as compared to detecting changes in mode shapes). Another advantage is that the wave travel time through the building can give the fundamental fixed-base frequency of a building, f_1, which is directly related to the stiffness of the structure, with minimum instrumentation, for example, with one sensor at the ground floor and another one at the roof [19]. On the other hand, the time frequency energy distributions yield the frequency of the soil–structure system, f_{sys}, which also depends on the stiffness of soil. Consequently, changes of f_{sys} have often been erroneously interpreted to be entirely due to loss of structural stiffness. For comprehensive and reliable structural health monitoring, it is essential to be able to monitor f_1 separately from f_{sys}.

DOI: 10.1002/stc

There have been only few publications on wave propagation methods, other than non-destructive testing (NDT), for structural health monitoring and damage detection in civil structures. Şafak [26] proposed a layered continuous model for analysis of seismic response of a building, and detection of damage by tracing changes in the parameters in the layers. Ivanović *et al*. [10] and Trifunac *et al*. [16] used strong motion data recorded in the Van Nuys during the 1994 Northridge earthquake to explore two methods, one based on cross-correlation analysis (to estimate time lags between motions recorded at different levels), and the other one based on detecting changes in wave numbers (inversely proportional to the wave velocities) of waves propagating between different levels. Ma and Pines [27] proposed a method based on a lumped mass building model, and propagation of dereverberated waves to identify the damage, which they tested on simulated building response data.

The wave propagation method applied in this paper, as well as the above-mentioned methods that use seismic monitoring data differ from the wave methods used in NDT of materials in that the latter typically use: (1) ultrasonic waves, which are attenuated quickly along the wave path; (2) need an actuator to create such waves; and (3) detect cracks, or some other defect in a member, using *reflected* waves from the defects. These methods are typically used locally, to detect the location of a defect in a member, but are impractical and too costly for global structural health monitoring [25]. The method in this paper uses seismic waves, which are long (5–500 m) and are not much attenuated, does not need actuators, and is based on measurements of travel times of waves *transmitted* through the damaged zone.

In this paper, we first present a brief description of the building, the available strong motion data, the reported damage, and results of ambient vibration tests (included for completeness of this presentation). Then the methodology is presented, and finally the results and the conclusions.

2. THE BUILDING

The building is located in central San Fernando Valley of the Los Angeles metropolitan area (at 34.221°N and 118.471°W), northwest from downtown Los Angeles. Figure 1 shows San Fernando Valley and the building location, relative to the major freeways and the horizontal projections of the fault planes of 1971 San Fernando and 1994 Northridge earthquakes [28, 29], the epicentres of two Northridge aftershocks, and directions and epicentral distances to seven other earthquakes recorded in the building [6].

The building was designed in 1965, and constructed in 1966 [1, 2]. Figure 2 shows (a) a plan view of a typical floor, (b) the foundation layout, (c) a side view of the building frame, and (d) a typical soil-boring log data at the building site. The building is 19.1×45.7 m in plan, and 20.03 m high. The typical framing consists of columns spaced at 6.35 m centres in the transverse direction, and 5.72 m centres in the longitudinal direction. Spandrel beams surround the perimeter of the structure. Lateral forces in each direction are resisted by interior column-slab frames and exterior column spandrel beam frames. The added stiffness in the exterior frames associated with the spandrel beams creates exterior frames that are roughly twice as stiff as the interior frames. The floor system is RC flat slab, 25.4 cm thick at the 2nd floor, 21.6 cm thick at the 3rd to 7th floors, and 20.3 cm thick at the roof. The properties of the construction materials are described in References [1, 18].

DOI: 10.1002/stc

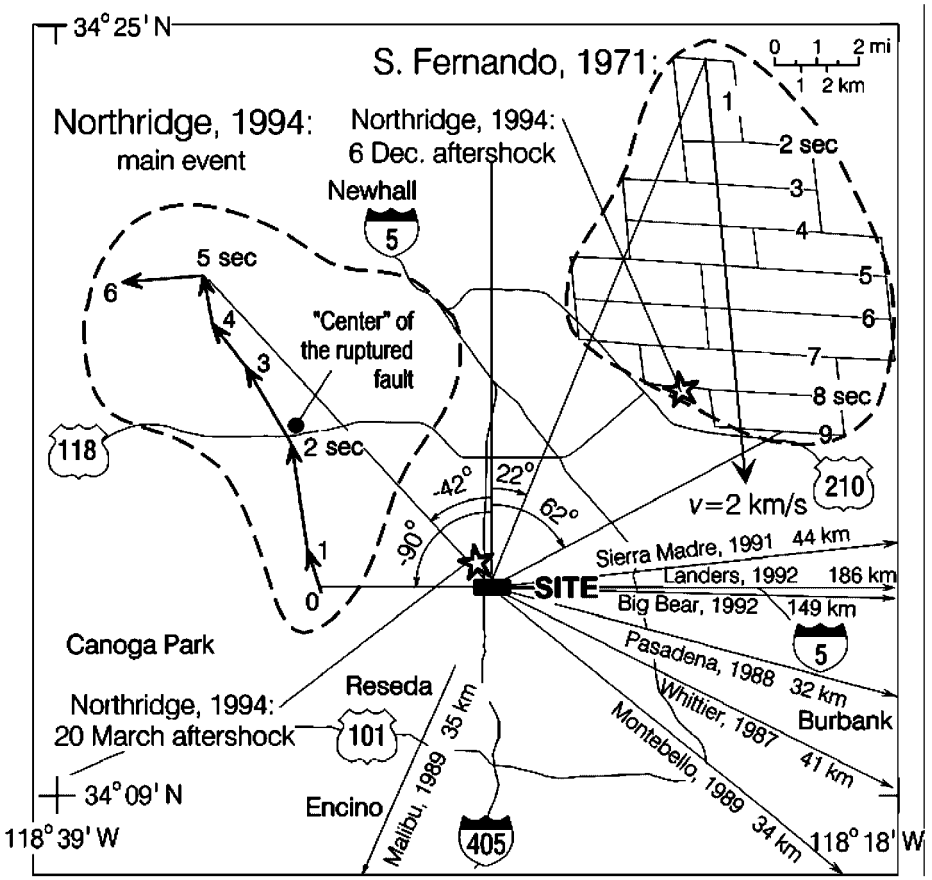

Figure 1. General setting of the Van Nuys building site in central San Fernando Valley. The location of the building relative to the fault planes of the 1971 San Fernando and 1994 Northridge earthquakes (their horizontal projections are shown by dashed lines), the epicentres of two Northridge aftershocks (solid stars), and other earthquakes with epicentres outside the map are also shown.

The building is situated on undifferentiated Holocene alluvium, uncemented and unconsolidated, with thickness <30 m, and age $<10\,000$ years, and average shear wave velocity in the top 30 m of soil of 300 m/s. The soil boring log in Figure 2(d) shows that the underlying soil consists primarily of fine sandy silts and silty fine sands. The foundation system (Figure 2(b)) consists of 96.5 cm deep pile caps, supported by groups of two to four poured-in-place 61 cm diameter RC friction piles, centred under the main building columns. The pile caps are connected by a grid of beams. The piles are 12.2 m long, and each has design capacity of over 444.82×10^3 N for vertical load, and up to 88.96×10^3 N for lateral load.

The $M_L = 6.6$ San Fernando earthquake of 9 February 1971 caused minor structural damage [1]. Epoxy was used to repair the spalled concrete of the second floor beam-column joints on the north side and east end of the building. The recorded peak accelerations in the building along the longitudinal (L), transverse (T), and vertical (V) axes of symmetry were: 0.13g (L), 0.24g (T), and 0.18g (V) at the base, and 0.32g (L), 0.39g (T), and 0.22g (V) at the roof.

DOI: 10.1002/stc

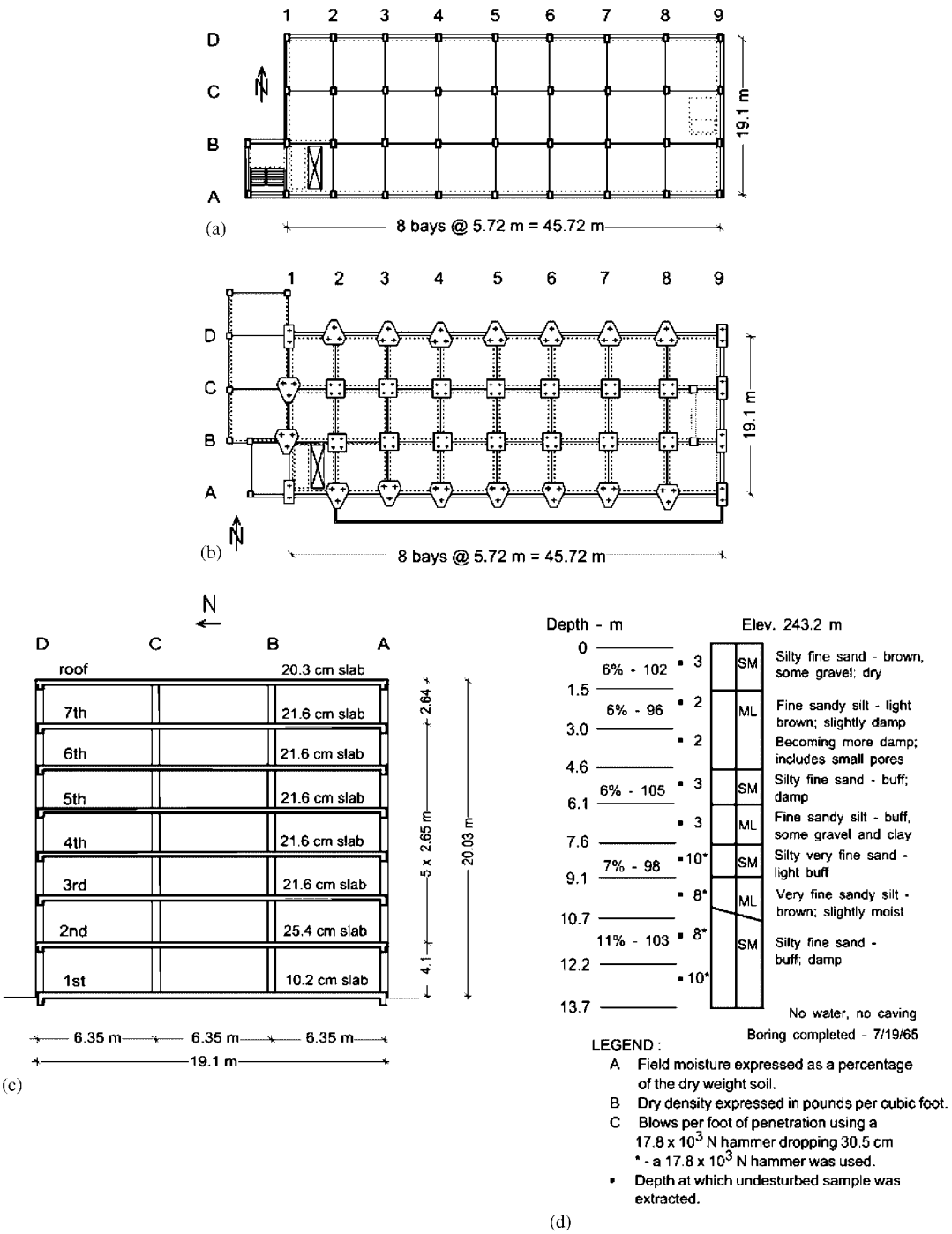

Figure 2. VN7SH building: (a) typical floor plan; (b) foundation plan; (c) typical transverse section; and (d) soil boring data from 17 July 1965.

DOI: 10.1002/stc

The $M_L = 6.4$ Northridge earthquake of 17 January 1994 severely damaged the building. The structural damage was extensive in the exterior north (D) and south (A) frames, designed to take most of the lateral load in the longitudinal (East-West (EW)) direction. Severe shear cracks occurred at the middle columns of frame A, near the contact with the spandrel beam of the 5th floor (Figure 3), which significantly decreased the axial, moment, and shear capacity of the columns. The shear cracks in the north (D) frame on the 3rd and 4th floors, and the damage of columns D2, D3, and D4 on the 1st floor caused minor to moderate changes in the capacity of these structural elements. No major damage of the interior longitudinal (B and C) frames was observed. There was no visible damage in the slabs and around the foundation. The nonstructural damage was significant. The recorded peak accelerations were as follows: 0.46*g* (L), 0.40*g* (T), and 0.28*g* (V) at the base, and 0.59*g* (L) and 0.58*g* (T) at the roof (there were no sensors installed on the roof to measure vertical motions). Photographs and detailed description of the damage can be found in References [6, 30].

2.1. Ambient vibration experiments

There have been five ambient vibration surveys of the Van Nuys building: (1) soon after construction, in 1967; (2) immediately following the San Fernando earthquake in 1971, before repair; (3) again in 1971, after repair [2]; (4) two and a half weeks after the Northridge earthquake, on 4 and 5 February 1994, before repair; and (5) one month following one of the largest aftershocks (of 20 March 1994, $M = 5.2$), on 19 and 20 April 1994 [5,8,9]. During the last two tests, detailed damage surveys were also conducted [6,30]. Between the two tests, wooden braces had been added near the areas of structural damage to increase the structural capacity. We do not know if there were braces at the time of the aftershock of 20 March 1994.

The first three tests [2] revealed that the first system frequency of EW response decreased from 1.89 Hz before the earthquake to 1.39 Hz following the earthquake (by 26%), and then increased to 1.56 Hz following the repairs (by 12%). For the NS response, it decreased from 2.08 Hz before the earthquake to 1.47 Hz after the earthquake (by 29%), and then increased to 1.72 Hz after repair (by 17%). During the fourth and fifth tests [8, 9], for the EW response, it was, respectively, 1.0 and 1.1 Hz, and for the NS response it was 1.4 Hz during both tests. The increase of the EW frequency by 10% is likely due to the addition of braces. We note that braces were added only to the longitudinal frames (at the first three or four stories at selected spans on the exterior frames, and at the first floor of the interior frames). Figure 4 shows the location of the braces in the exterior frames (the size of the 'hinges' is proportional to the level of damage). We also note that an increase of the width of the cracks was observed during the last tests, especially in the south (A) frame, but no new structural damage.

2.2. Strong motion records

The 12 earthquakes for which strong motion data were available for this analysis are listed in Table I, along with their magnitude, M, and epicentral distance, R. Their epicentres, or direction and distance to their epicentres are shown in Figure 1. The instrumentation originally consisted of three self-contained tri-axial AR-240 accelerographs, which recorded the 1971 San Fernando earthquake, and was later replaced by a 13 channel CR-1 central recording system and a tri-axial SMA-1 accelerograph, which recorded the other events. The sensor locations are shown in Figure 5. The film records of the San Fernando earthquake were digitized manually, with

DOI: 10.1002/stc

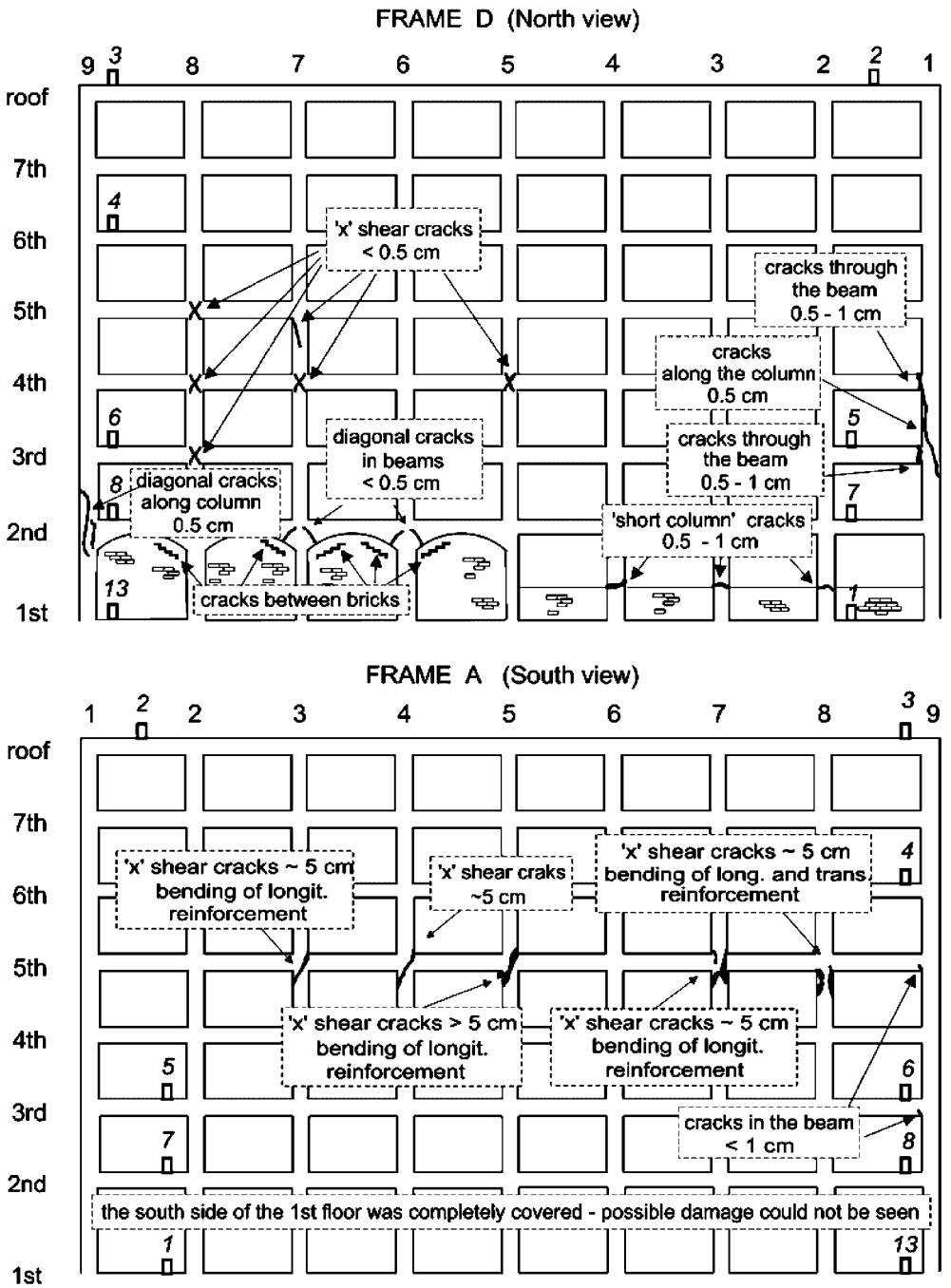

Figure 3. Schematic representation of the damage: (top) frame D—north view, and (bottom) frame A—south view. The sensor locations for channels 1–8 and 13 (oriented towards north) are also shown.

DOI: 10.1002/stc

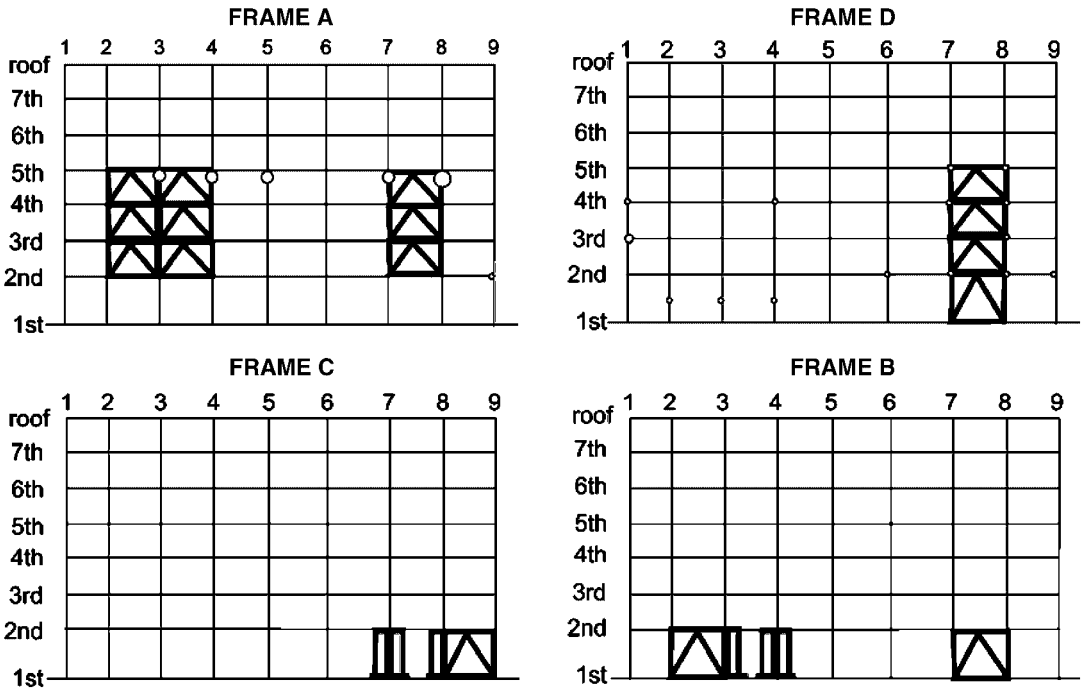

Figure 4. Location of the braces, and schematic representation of the damage (shown by circles with size proportional to the damage) observed during the last ambient vibration experiment on 19 April 1994.

Table I. Earthquakes recorded in the Van Nuys building for which digitized data are available.

No.	Earthquake	Date	M	R (km)
1	San Fernando	09/02/1971	6.6	22
2	Whittier Narrows*	01/10/1987	5.9	41
3	Whitter-Narrows aft.	04/10/1987	5.3	38
4	Pasadena	03/10/1988	4.9	32
5	Montebello	12/06/1989	4.1	34
6	Malibu	19/01//1989	5.0	36
7	Sierra Madre	28/06/1991	5.8	44
8	Landers	28/06/1992	7.5	186
9	Big Bear	28/06/1992	6.5	149
10	Northridge	17/01/1994	6.5	1.5
11	Northridge aft.	20/03/1994	5.2	1.2
12	Northridge aft.	06/10/1994	4.5	10.8

*EW component of accelerograph on ground floor malfunctioned, and the record is not available. Hence, this event is not included in the present analysis.

sampling > 50/s [31]. The records of the other larger events (Nos. 2, 8, 9, 10, and 11 in Table I) were digitized and released by California Geological Survey (CGS; formerly California Division of Mines and Geology), which operates the instrumentation [32]. The records of the smaller

DOI: 10.1002/stc

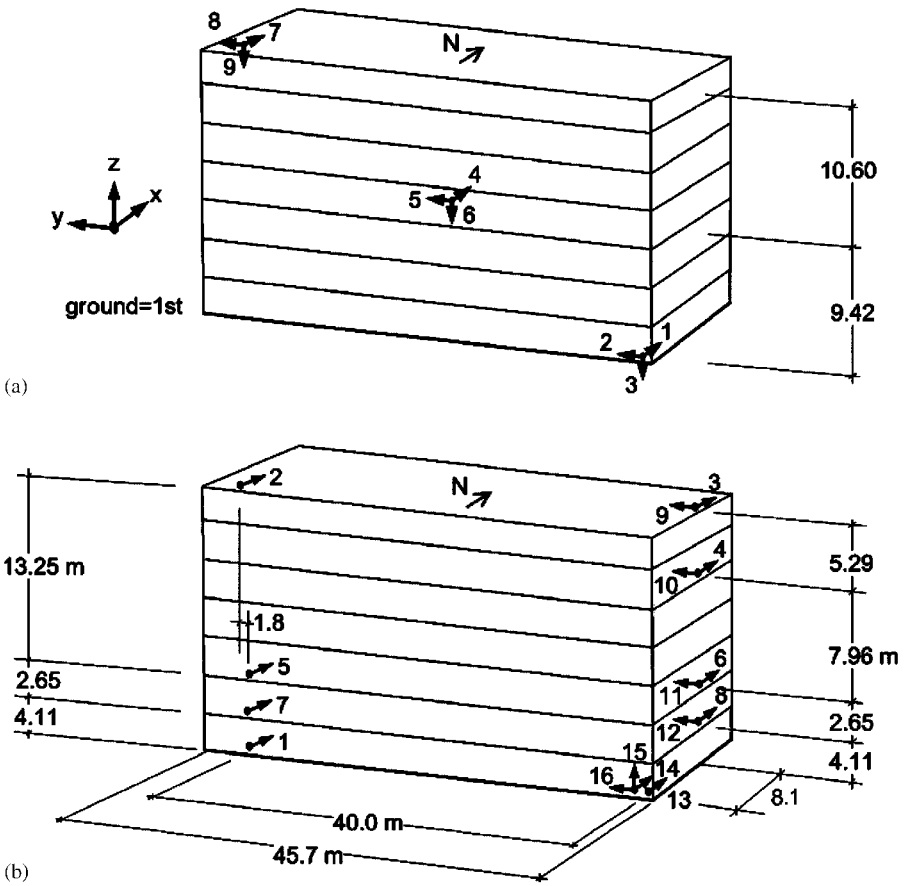

Figure 5. Location of (a) the three AR-240 accelerographs, which recorded the San Fernando, 1971 earthquake, and of (b) the 13 channels of the CR-1 recording system, and the SMA-1 accelerograph (channels 14–16), which recorded all earthquakes between mid-1970s and 1994.

events (Nos. 3–7, and 12 in Table I) were digitized at the University of Southern California from photocopies in published reports or provided by CGS (event No. 12; Graizer, personal communication, 1997; [33]). Other events might have also been recorded in the building, such as other aftershocks of the Northridge earthquake.

3. METHODOLOGY

The methodology is based on a 1D continuous shear wave propagation model of the building lateral response, and measuring wave travel times from impulse response functions computed by deconvolution. The following describes the building model, how travel times are measured, how the building fixed-base frequency is estimated using data from only two sensors, and the structural health monitoring scheme.

DOI: 10.1002/stc

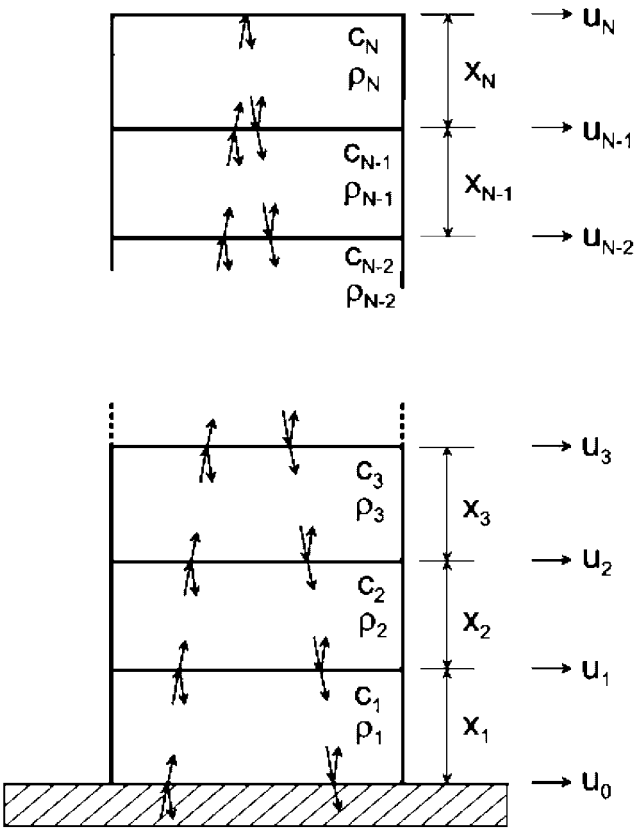

Figure 6. The model.

3.1. *Wave propagation model*

The conceptual model we consider is a layered shear beam, shown in Figure 6, with the interfaces between layers at the floor slabs, and the variations of the layer properties depicting variations in floor stiffness and mass along the building height. In this figure, c_i, ρ_i, and x_i represent the shear wave velocity, mass density, and height of layer i, and u_i is the displacement at the top of the layer. An incident seismic wave train (ray) would be partly transmitted into the building and partly reflected back into the soil. The transmitted wave would also be partly transmitted and partly reflected at each interface. The transmitted (upward propagating) wave will be delayed and attenuated along the wave path. The transmitted wave into the last (top) layer will be totally reflected back from the stress-free top surface. The downward propagating wave would also be partly transmitted in the lower layer and partly reflected back at each of the interfaces, and will be further delayed and attenuated along the wave path. When this wave reaches the interface with the soil, it will be partly reflected back into the building and partly transmitted out into the soil. The process then repeats infinitely many times, in theory, and practically until all waves are attenuated. Such partial transmission and reflection will occur also

DOI: 10.1002/stc

for the reflected waves. To avoid clutter, Figure 6 shows only the first generation transmissions and reflections.

The earthquake ground motion consists of many such wave trains that hit the building with some time delay relative to the first arrival. Then, the resulting motion is a superposition of infinitely many waves propagating upwards and downwards. For example, at each instant, the resulting upward propagating wave at the interface with the soil is a superposition of the direct wave train just transmitted from the soil into the building, and all waves in the bottom layer just reflected back into the building, resulting from different generations of reflections. The infinite sum of wave trains parallels the representation of the response as an infinite sum of modal responses. Such a model of building seismic response in its simplest form—a uniform shear beam—has been considered earlier by Kanai [34], who presented simple formulae for the infinite sums, and recently by Snieder and Şafak [19], who also showed the equivalence of the two representations. The strong ground motion consists of pulses, representing bursts of energy that enter the building. Such pulses can be traced by a naked eye in some strong motion records in tall buildings, but only in the initial stages of response, before standing waves resulting from constructive interference of the waves trapped into the building start dominating the response.

In this paper, we measure wave travel times by tracing a single input pulse created by signal processing of the recorded accelerograms. In particular, we compute impulse response functions by deconvolution of the response recorded at different stories [19,21], as follows. Let us assume that the building is a linear time-invariant system, over the entire duration or a segment of the earthquake shaking. This system has a single input $u_{\text{ref}}(t)$ (the motion at some reference point) and multiple outputs $u_i(t)$ (Figure 6). The input and outputs are related in the time and frequency domains by

$$\begin{aligned} u_i(t) &= (u_{\text{ref}} * h_i)(t) \\ &= \int_0^t u_{\text{ref}}(\tau) h_i(t-\tau)\,\mathrm{d}\tau \quad \Leftrightarrow \quad \hat{u}(\omega) = \hat{u}_{\text{ref}}(\omega)\hat{h}_i(\omega) \end{aligned} \tag{1}$$

where $*$ indicates convolution, and the hat indicates Fourier transform. Further, $h_i(t)$ and $\hat{h}_i(\omega)$ represent the system function in the time and frequency domains. Physically, $h_i(t)$ represents the output (response at level i) when the input (i.e. $u_{\text{ref}}(t)$) is a Dirac delta function (in discrete time that would be the unit impulse function). Indeed, at the reference point, the transfer function is equal to unity, the inverse Fourier transform of which is the Dirac delta function. Any point can be used as reference, not just the base, in which case $h_i(t)$ represents the motion at level i if the motion at the reference point is the unit impulse function. Hence, the propagation of a single impulse through the building can be traced by computing $h_i(t)$ given $u_{\text{ref}}(t)$ and $u_i(t)$, i.e. by deconvolution of the recorded building response. This can be practically done by computing inverse Fourier transform of the corresponding transfer functions. To avoid singularities, we compute $h_i(t)$ as

$$h_i(t) = \mathrm{FT}^{-1}\left\{\frac{\hat{u}_i(\omega)\overline{\hat{u}}_{\text{ref}}(\omega)}{|\hat{u}_{\text{ref}}(\omega)| + \varepsilon}\right\} \tag{2}$$

where the bar indicates complex conjugate, and ε is a regularization parameter [19]. Then we measure the pulse arrival time directly from the waveform, assuming that its shape is defined mostly by the transmitted waves through the layers, and is not much influenced by reflections from the boundaries of impedance contrast, or the sides of the building.

DOI: 10.1002/stc

3.2. Estimation of fixed-base frequency

If the building response is predominantly 1D, the point of fixity is at ground level, and the deformations are mainly in shear, then the wave travel time from the base to the roof, τ_{tot} , is $\frac{1}{4}$ of the fundamental *fixed-base* period of vibration T_1, and the fundamental fixed-base frequency is

$$f_1 = 1/(4\tau_{tot}) \tag{3}$$

Snieder and Safak [19] examined the effect of coupling with the soil on the wave travel time and estimate of f_1. In their model, the soil is just like another layer of the building deforming in shear only. They showed that, for such a model, the travel time of the impulse is not affected by the coupling with the soil. However, such a model does not consider the foundation rocking, which occurs in the in-plane response soil–structure interaction problem [35, 36]. For example, buildings on rigid embedded foundations that are excited by general in-plane wave motion not only deform but also move as a rigid body (translate and rotate). The motions of the upper floors due to the rigid body rocking cannot be separated from those due to deformation of the building even in the most ideal case of a relatively stiff base and floor slabs unless there are at least two vertical sensors at the base. That was not the case for the Van Nuys building, as well as for most instrumented building. In our analysis, we assume that the rigid body rocking affects mostly the peak amplitude of the propagating pulse, but not the shape of the pulse—hence the reading of the pulse arrival time—and that the associated errors are within the 'noise' level (i.e. errors due to all other simplifying assumptions).

For buildings on flexible soil, the energy of the relative response is concentrated around the frequencies of the soil–structure system, which are different from the building fixed-base frequencies. Let f_{sys} be the lowest such frequency (a result of coupling with f_1). Then f_{sys} and f_1 are related by

$$f_{sys}^{-2} = f_1^{-2} + f_H^{-2} + f_R^{-2} \tag{4}$$

where f_H and f_R represent the horizontal and rocking frequencies of a rigid building on flexible soil. Equation (4) implies that always $f_1 > f_{sys}$. Our analysis of the Imperial County Services building [21]—a building damaged by the 1979 Imperial Valley earthquake to which the same method as in this paper was previously applied—showed that f_1, as estimated from impulse response analysis, was always higher than f_{sys}, as estimated from a time–frequency energy distribution (specifically, from the ridge of the Gabor transform of the relative roof displacement response), which supports the hypothesis that f_1 is approximately the fixed-base frequency. In this paper, we further examine this hypothesis by checking this relationship for 11 events recorded in the Van Nuys building, and by analysing variations in f_1 and their correlation with earthquake damage.

3.3. Structural health monitoring

Global changes in the structural stiffness will be monitored by detecting changes in the total wave travel time along the building height (equivalent to monitoring changes in the equivalent shear wave velocity, v_{eq}, or f_1), and local changes will be monitored by detecting changes in wave travel time between sensors at different floors. Changes will be detected by measuring the travel times in consecutive time windows during the earthquake shaking, and comparing the values with those for the initial time window. Eventually, a sliding window can be used and 'instantaneous' travel times can be measured. Such a scheme does not need baseline data

DOI: 10.1002/stc

measured before the earthquake, and is not sensitive to permanent or temporary changes in the structure not related to damage [25]. We used earlier this scheme in our analysis of the Imperial County Services building [21].

4. RESULTS AND ANALYSIS

We present results only for the EW (longitudinal) response, which is less affected by torsion, and hence is more suitable for modeling by a 1D wave propagation model. Also, the observed damage appears to have been caused mainly by EW deformations. An analysis of the NS response would be more complex requiring simultaneous consideration of large rocking, coupled with torsion, and will be addressed in our future work. We used data from 11 earthquakes. In the following, we present results for the impulse responses, f_1 and its relation to f_{sys}, shear wave velocities between floors and inferred changes of floor stiffness, and plots of different quantities involving f_1 and selected parameters of the recorded response. Finally, we discuss the threshold changes indicative of structural damage.

4.1. Impulse responses for EW motions

Figures 7–9 show impulse response functions for the three largest events (1971 San Fernando, 1992 Landers, and 1994 Northridge earthquakes; see Reference [18] for such plots for the eight smaller events). The different types of lines correspond to different time windows. The plots on the left-hand side correspond to an input impulse at the ground floor, and those on the

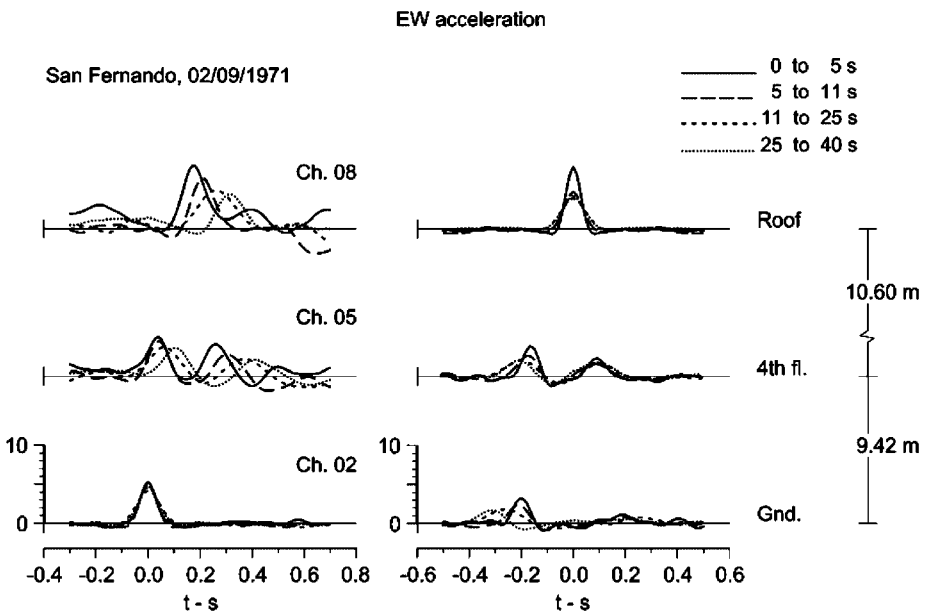

Figure 7. Impulse response functions for EW motion of the Van Nuys building during the 1971 San Fernando earthquake.

DOI: 10.1002/stc

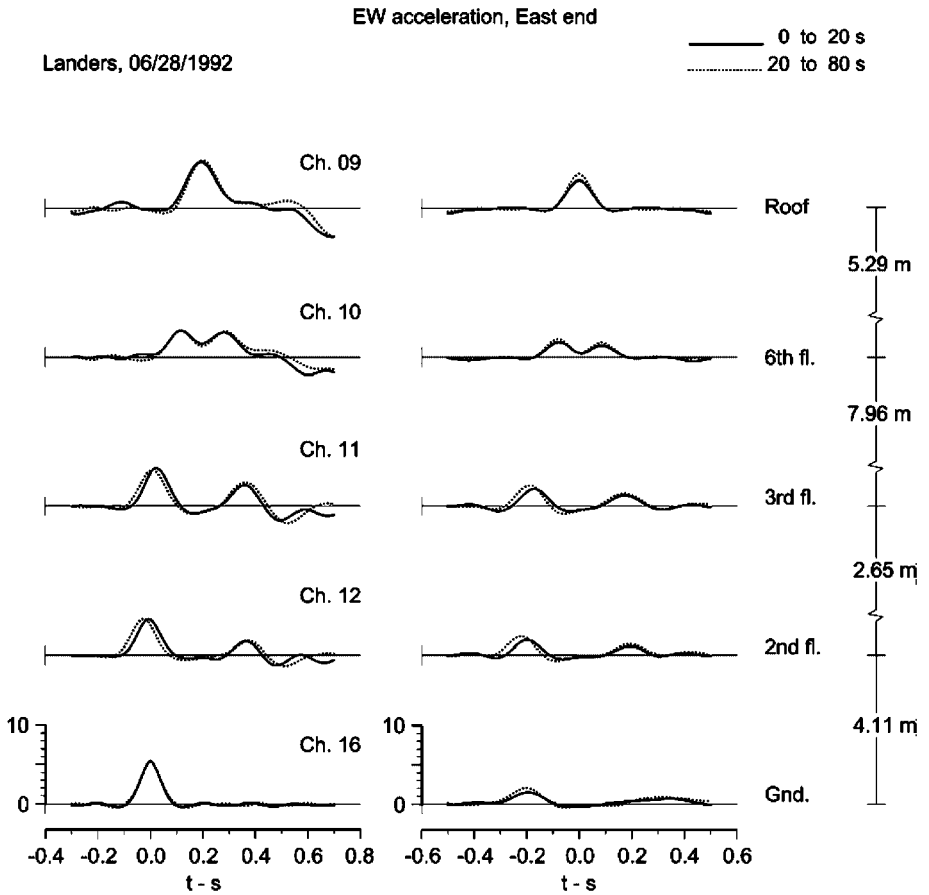

Figure 8. Same as Figure 7 but for the 1992 Landers earthquake.

right-hand side to an input impulse at the roof. These are shown only for the early stages of response to emphasize the arrival times of the primary pulses. The input pulse has a finite width because of the windowing in time (i.e. finite duration of the records), and also due to the regularization parameter ε. We used $\varepsilon = 0.1 * \bar{P}$ when u_{ref} is the ground floor record, and $\varepsilon = 0.05 * \bar{P}$ when u_{ref} is the roof record, where $\bar{P}$ is the average power of u_{ref}. One can see from the plots on the left how the input impulse at the ground floor propagates up, arriving with some time delay at the upper floors, and then propagates down after reflection from the roof. In the plots on the right, one can see the input impulse at the roof, which propagates down causally (in positive time), and also acausally (in negative time). The acausal wave corresponds to a wave propagating up in the physical model.

The pulse arrival times can be read clearly for: (i) the direct wave going up—when the input impulse is at the base; and (ii) the direct acausal wave going down—when the input impulse is at the roof. In our analysis, we used the *mean* of the travel times estimated from these two pulses. Tables with readings of the arrival times for these two pulses, their mean values, and the inferred

DOI: 10.1002/stc

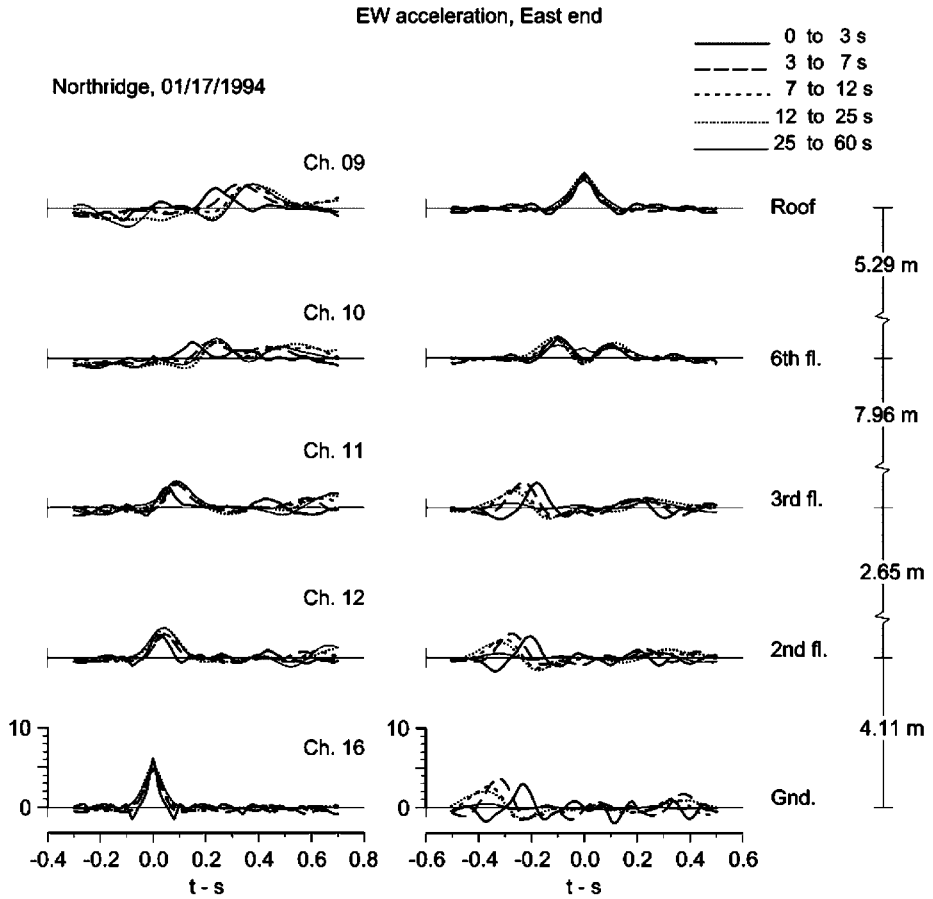

Figure 9. Same as Figure 7 but for the 1994 Northridge earthquake.

wave velocities can be found in Reference [18]. In this paper we only show tables for the global properties. Table II shows, for all 11 events, the (mean) *total* travel times along the height of the building, τ_{tot}, the corresponding estimates of equivalent uniform shear wave velocity, v_{eq}, and the fundamental fixed-base frequency, f_1. For the San Fernando, Landers, and Northridge earthquakes, results are also shown for the percentage changes in wave velocity and in shear moduli, relative to the respective initial time interval. Table III shows also f_1 along with some basic parameters of the recorded response during the 11 events. Columns (1) and (2) show the code identifying the event/segment (same as in Column (1c) of Table II), and the corresponding estimate of f_1. Columns (3a)–(3d) show, respectively, the peak ground acceleration $a_{\max}^{\text{Gnd}}$, peak roof acceleration $a_{\max}^{\text{Roof}}$, peak ground velocity $v_{\max}^{\text{Gnd}}$, and the peak roof relative displacement $d_{\max}$. Columns (3e)–(3h) show some quantities derived from the values shown in the preceding columns, in particular, they show the average value of the ground and roof peak accelerations $\bar{a}_{\max} = (a_{\max}^{\text{Gnd}} + a_{\max}^{\text{Roof}})/2$, $d_{\max}\omega_1^2$, f_1^2 and $v_{\max}^{\text{Gnd}}/(4f_1)$.

DOI: 10.1002/stc

Table II. Equivalent shear wave velocities of a uniform shear beam, v_{eq}, and fundamental fixed-base frequencies of vibration, f_1, estimated from the mean wave travel times τ_{tot} over the building height, for EW motions and for all 11 events and time windows considered.

				EW motions				
(1a) Earthquake	(1b) Date	(1c) Segment	(1d) Time interval (s)	(2a) τ_{tot} (s)	(2b) v_{eq} (m/s)	(2c) f_1 (Hz)	(2d) $\Delta f_1/\Delta f_{1,ref}$ (%)	(2e) $\Delta\mu_1/\Delta\mu_{1,ref}$ (%)
San Fernando	09/02/1971	S1	$t<5$	0.185	108.2	1.35		
		S2	$5<t<11$	0.2025	98.9	1.23	−9	−16
		S3	$11<t<25$	0.255	78.8	0.98	−27	−47
		S4	$25<t<40$	0.305	65.7	0.82	−39	−63
Whitter-aft.	04/10/1987	WA	$t<24$	0.2075	96.5	1.20		
Pasadena	03/10/1988	PA	$t<24.5$	0.205	97.7	1.22		
Malibu	19/01//1989	MA	$t<25$	0.209	95.8	1.20		
Montebello	12/06/1989	MB	$t<24$	0.1925	104.0	1.30		
Sierra Madre	28/06/1991	SM	$t<23$	0.2175	92.0	1.15		
Landers	28/06/1992	L1	$t<20$	0.1975	101.4	1.27		
		L2	$20<t<80$	0.205	97.7	1.22	−4	−7
Big Bear	28/06/1992	BB	$t<40$	0.215	93.1	1.16		
		N1	$t<3$	0.295	67.9	0.85		
		N2	$3<t<7$	0.325	61.6	0.77	−9	−18
Northridge	17/01/1994	N3	$7<t<12$	0.365	54.8	0.68	−19	−35
		N4	$12<t<25$	0.38	52.7	0.66	−22	−40
		N5	$25<t<60$	0.38	52.7	0.66	−22	−40
Northridge aft.	20/03/1994	A1	$t<26$	0.31	64.6	0.81		
Northridge aft.	06/10/1994	A2	$t<26$	0.27	74.1	0.93		

For the San Fernando, Landers, and Northridge earthquakes, the percentage change in f_1 and the equivalent rigidity are also shown.

4.2. *Changes of f_1 and comparison with f_{sys}*

It can be seen from Table II that v_{eq} varied between 108 m/s during the first time interval of the San Fernando earthquake ($t<5$ s) and 53 m/s during the Northridge earthquake ($12<t<60$ s), which corresponds to $f_1 = 1.35$ Hz and 0.66 Hz. As v_{eq} and f_1 are directly related ($f_1 = v_{eq}/(4H)$), we analyse only f_1.

Figure 10 shows f_1 and f_{sys} *versus* time during the 11 earthquakes (see Table I and Figure 1), and also f_{sys} during the five ambient vibration tests. The curves for f_1 are hand interpolations/extrapolations of the interval values (shown by open circles) assigned to the central time of the intervals. The curves for f_{sys} are smooth values obtained from the ridge of the Gabor transform, after eliminating some variations believed to be due to artefacts [22]. In real life signals, the artefacts are largely due to violation of the assumption that the signal is asymptotic, which refers to signals that vary in time mostly due to change of phase, while the variation of their amplitude envelope is small [37]. The assumption of asymptoticity is common to virtually all methods used for estimation of instantaneous frequency using time–frequency or time-scale energy distributions (e.g. the moving window analysis, the continuous complex wavelet transform, Vigner–Ville transform, etc. [37]). Violations of this assumption (i.e. rapid variations of the amplitude envelope during one cycle of vibration) lead to large apparent variations of the instantaneous frequency, which are not true. Other artefacts are due to small signal to noise

DOI: 10.1002/stc

Table III. Values of f_1, estimated from the mean wave travel times, and selected recorded motion parameters for the 19 segments analysed.

	EW motions								
(1) Segment	(2) f_1 (Hz)	(3a) $a_{\max}^{\text{Gnd}}$ (cm/s^2)	(3b) $a_{\max}^{\text{Roof}}$ (cm/s^2)	(3c) $v_{\max}^{\text{Gnd}}$ (cm/s)	(3d) $d_{\max}$ (cm)	(3e) $\bar{a}^*_{\max}$ (cm/s^2)	(3f) $d_{\max}\omega_1^2$ (cm/s^2)	(3g) f_1^2 (Hz^2)	(3h) $v_{\max}^{\text{Gnd}}/(4f_1)$ (cm)
S1	1.35	119.74	186.78	9.12	1.84	153.26	132.16	1.82	1.69
S2	1.23	129.97	315.30	13.02	4.49	222.64	267.71	1.51	2.65
S3	0.98	118.39	289.14	22.38	7.75	203.76	293.52	0.96	5.71
S4	0.82	23.57	59.87	6.68	2.12	41.72	56.17	0.67	2.04
WA	1.20	52.43	53.59	2.18	0.89	53.01	50.81	1.44	0.45
PA	1.22	32.72	29.92	0.94	0.40	31.32	23.53	1.49	0.19
MA	1.20	19.83	28.20	0.93	0.32	24.01	18.00	1.44	0.19
MB	1.30	21.33	27.36	0.80	0.18	24.35	11.95	1.69	0.15
SM	1.15	62.05	57.90	2.76	1.41	59.97	73.58	1.32	0.60
L1	1.27	28.22	125.02	5.25	2.93	76.62	186.16	1.61	1.03
L2	1.22	39.97	116.79	10.26	3.18	78.38	186.91	1.49	2.10
BB	1.16	23.48	54.18	3.02	1.60	38.83	84.64	1.35	0.65
N1	0.85	97.77	104.33	5.80	2.00	101.05	57.11	0.72	1.71
N2	0.77	389.34	435.78	39.61	16.34	412.56	381.97	0.59	12.86
N3	0.68	442.22	563.20	51.06	22.64	502.71	412.88	0.46	18.77
N4	0.66	187.86	232.62	25.90	13.61	210.24	233.73	0.44	9.81
N5	0.66	42.78	233.21	9.30	14.51	137.99	249.35	0.44	3.52
A1	0.81	137.18	89.98	4.86	1.10	113.58	28.43	0.66	1.50
A2	0.93	60.36	37.53	2.26	0.68	48.95	23.30	0.86	0.61

$*\bar{a}_{\max} = (a_{\max}^{\text{Gnd}} + a_{\max}^{\text{Roof}})/2$.

ratio in the beginning of the excitation [22]. The variations of the amplitude envelopes for the signals analysed in this paper can be seen from the plots of the relative roof displacement response, shown in Figure 10 above the plots showing the variations of frequency.

Figure 10 shows that f_1 and f_{sys} are the lowest during the largest earthquake shaking, and that $f_{\text{sys}} < f_1$ during all the earthquakes, consistent with Equation (4). However, *their ratio is not uniform*, as suggested by Equation (4), which describes a *linear* model. Between 1987 (Whittier aftershock) and 1992 (Big Bear earthquake), while f_1 is approximately constant for all events, fluctuating around 1.2 Hz, f_{sys} changed significantly from one earthquake to another, and relative to f_1. Its large fluctuations, between about 0.7 Hz (second segment of Landers earthquake) and 1.1 Hz (Malibu earthquake), are obviously not related to damage. Therefore, f_{sys} should not be used for structural health monitoring and damage detection.

Figure 10 shows that f_{sys} during ambient tests is always significantly higher than f_{sys} during earthquake shaking, confirming the strong amplitude dependence of f_{sys} on the level of the excitation known from numerous other tests [e.g. 38, 39]. The particularly high value of f_{sys} during the ambient tests in 1967 (one year after construction and before any exposure to strong earthquake shaking) could be explained by the fact that the concrete in the structural members was 'not cracked'—hence, the columns and beams worked with their almost gross moments of inertia. This all changed permanently during the San Fernando earthquake.

One can also see from Figure 10 that f_{sys} during ambient tests is higher than f_1 during the earthquake shaking, which is in contradiction with Equation (4). For example, f_{sys} during the ambient test after the San Fernando earthquake and before repair is larger by 0.57 Hz (41%)

DOI: 10.1002/stc

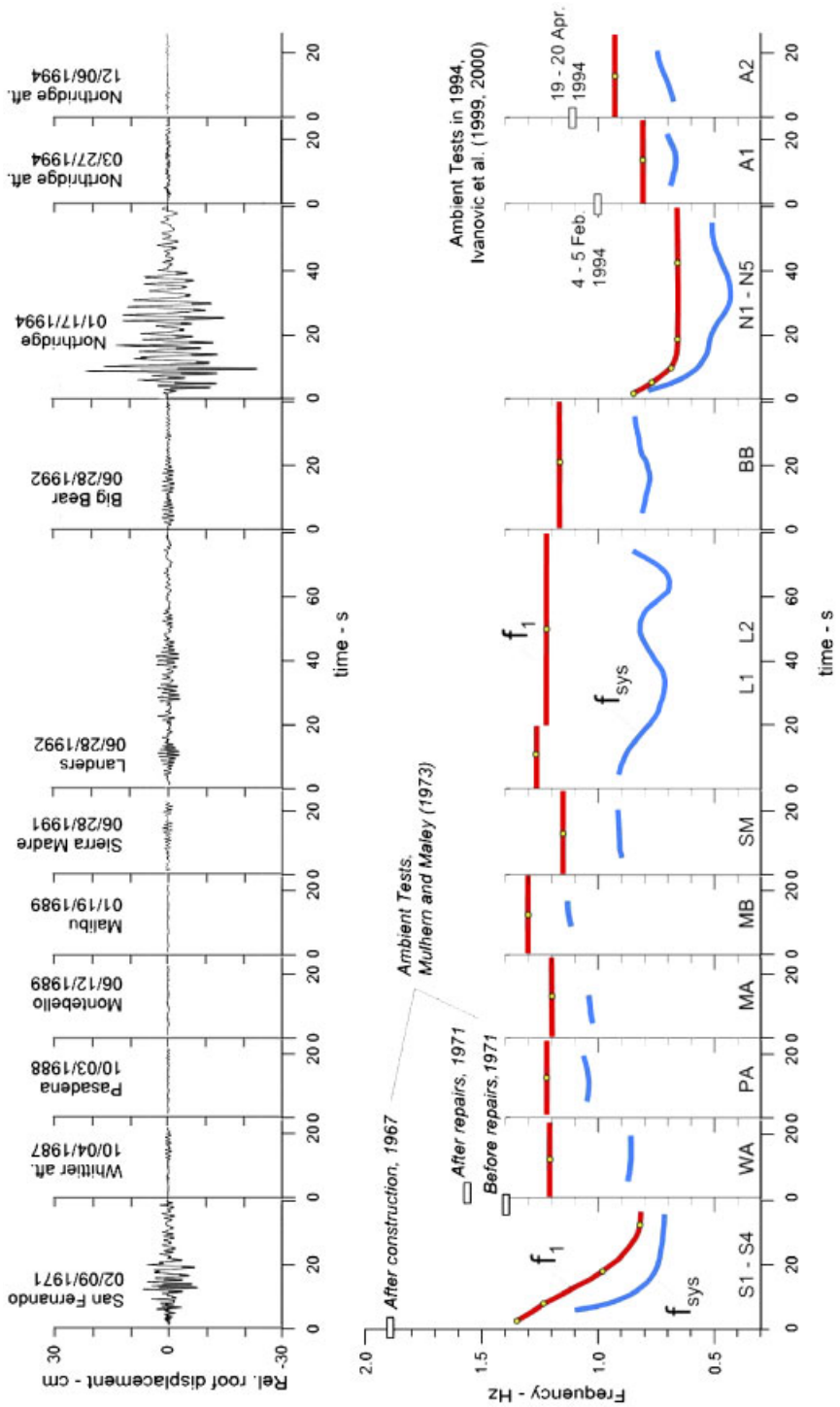

Figure 10. Variations of f_1 and f_{sys} in the Van Nuys building during the 11 earthquakes, between February 1971 and December 1994. Measured values of f_{sys} during five ambient vibration tests: (i) in 1967, following construction; (ii) in 1971, after San Fernando earthquake and before repairs; (iii) in 1971 after the repairs [2]; (iv) in January of 1994, 18 days after the Northridge earthquake; and (v) in April of 1994, after the building was restrained by wooden braces [8, 9].

DOI: 10.1002/stc

than f_1 near the end of the earthquake shaking (interval $25 < t < 40$ s). After the repairs, f_{sys} under ambient load increased by 0.17 Hz (by 12%). A similar relationship is seen for the tests conducted after the Northridge earthquake; however, the difference between f_1 near the end of the earthquake shaking and f_{sys} during the following ambient test before repair is much smaller. After adding the wooden braces, f_{sys} under ambient loads increased by 0.1 Hz (10%).

The higher values of f_{sys} during ambient tests than f_1 during earthquake shaking, which is in contradiction with the relationship between the two frequency described by Equation (4), based on linear theory, suggests strong dependence of f_1 on the amplitude of response. One possible cause for this dependence is the additional stiffness from the non-structural elements (e.g. partition walls) during ambient vibrations loads, which become 'loosely' connected to the structural elements during earthquake loads, and hence do not contribute to the structural stiffness. Another possible cause for the (recoverable) nonlinear behaviour is opening of existing cracks in the concrete during earthquake response.

4.3. Changes of average floor velocities and stiffness

The average floor velocities between sensors, v_i, represent local properties of the building. We computed v_i from the mean wave travel time between sensors, τ_i, and the distance between sensors, h_i, as $v_i = h_i/\tau_i$, and they represent average values for floors between the sensors. Figure 11 shows the variations of v_i during the 11 earthquakes. Due to the

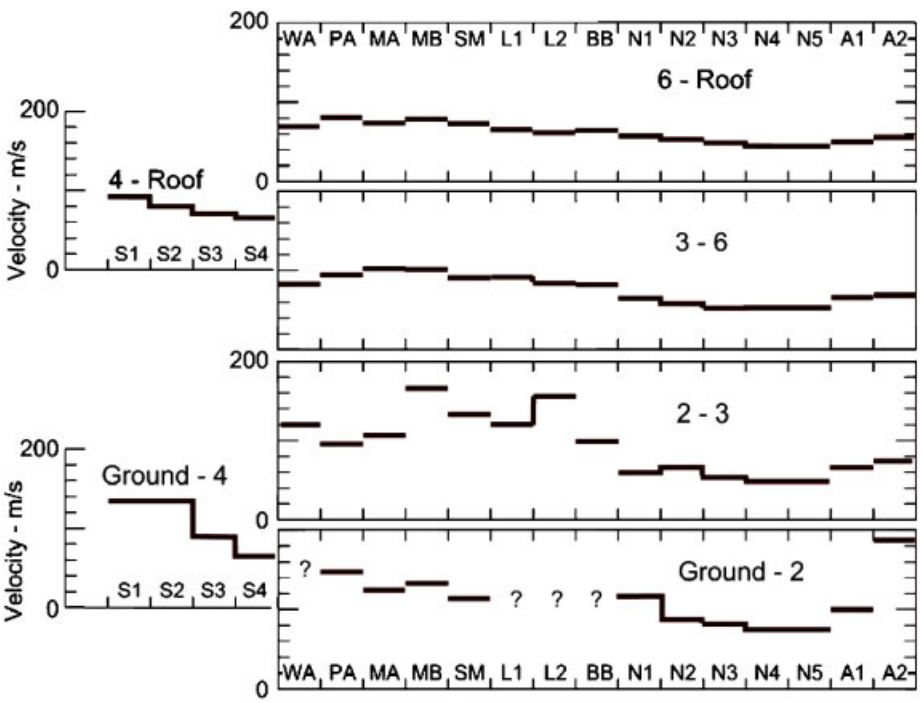

Figure 11. Average shear wave velocities between floors in the Van Nuys building during the 11 earthquakes. The different events and time intervals of the two largest events are identified by a code (see Table II for identification of the events and time segments).

DOI: 10.1002/stc

particular sensor location (see Figure 5), for the San Fernando earthquake, v_i is shown only for two segments along the building height—ground to 4th floor, and 4th floor to roof, and for all other events it is shown for four segments—ground to 2nd floor, 2nd to 3rd floors, 3rd to 6th floors, and 6th floor to roof. It can be seen from Figure 11 that, during the strong motion segment of San Fernando earthquake ($t < 30$–40 s), v_i between the ground and 4th floor dropped from near 140 m/s to about 70 m/s (−50%). Above the 4th floor, the relative drop of v_i was smaller, from about 90 to 70 m/s (−22%). The shaking amplitudes during the period from 1987 to 1992 were small and, except perhaps for the LA event, the building responded in an essentially linear manner. As Figure 11 shows, during this time v_i fluctuates, which we interpret to be mainly due to errors in the manual reading of the arrival times, for impulses propagating up and down the building, and due to undocumented changes in the building environment (e.g. [30]). These fluctuations are larger for the lower floors, for which the relative error in the estimation of the travel times was larger (due to the smaller distance between sensors). For that reason, the velocities between the ground and 4th floor are not shown for the WA, L1, L2, and BB events, as unreliable. The accuracy of the estimated propagation times can be improved by modelling in terms of ray tracing in the building, but this is beyond the scope of this analysis.

The average wave velocities experienced another significant drop during the Northridge earthquake in 1994. Between the ground and 2nd floor, for example, the velocity dropped from about 120 to near 70 m/s (−40%). We believe this drop is a result of the damage in the building (Figures 3 and 4). Figure 11 shows an increase in the wave velocities throughout the building during the two Northridge aftershocks, which we believe is a consequence of the increase in stiffness due to the wooden braces. These braces were added following the earthquake, to strengthen the building until completion of the repairs in 1996 (see Figures 3 and 4; [30]).

Figure 12 shows normalized floor shear wave velocities, v_i/v_{ref}, and rigidities, μ_i/μ_{ref}, *versus* time during the 1971 San Fernando and Northridge earthquakes, where v_{ref} and μ_{ref} are the values for the corresponding initial time intervals. These were computed from the travel times as $v_i/v_{\text{ref}} = \tau_{\text{ref}}/\tau_i$ and $\mu_i/\mu_{\text{ref}} = (\tau_{\text{ref}}/\tau_i)^2$, assuming almost uniform distribution of mass density along the building height. It can be seen from this figure that, during the San Fernando earthquake, the large drop in stiffness occurred gradually—over a period of 30 s, while, during the Northridge earthquake, this drop was rapid—over a period of 10 s. The drop of stiffness was the largest in the lower floors for both earthquakes (by about 80% between the ground and 4th floor during the San Fernando earthquake, and by about 60% between the ground and 2nd floor during the Northridge earthquake). The reductions in stiffness at higher elevations in the building were smaller (by about 50% during the San Fernando and by about 30–40% during the Northridge earthquake).

The observed damage in the building following the Northridge earthquake was more severe than during the San Fernando earthquake, contrary to the relative drop in stiffness implied by the analysis of travel times. We interpret this to be due to the fact that the building was already weakened at the time of the Northridge earthquake, by repeated shaking from the previous earthquakes. Although the building was repaired after the San Fernando earthquake, numerous small cracks remained, which were reactivated and enlarged by the subsequent earthquakes between 1987 and 1992. Thus, the severe damage occurred during the Northridge earthquake with smaller relative reduction of stiffness.

DOI: 10.1002/stc

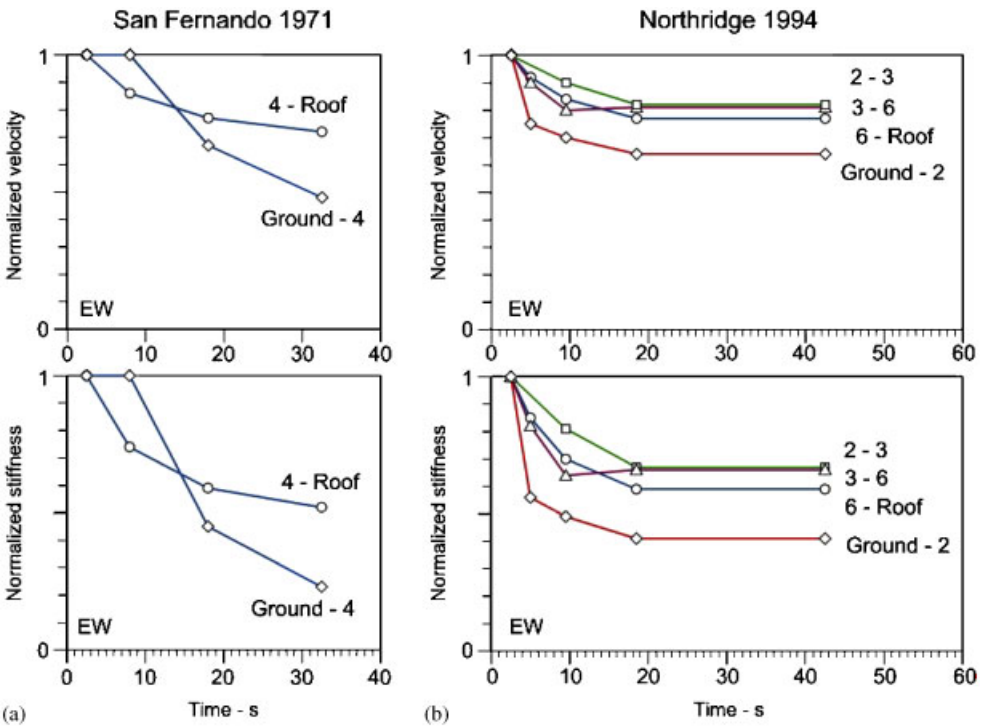

Figure 12. Reduction of the average wave velocities (top) and stiffness (bottom) between floors during: (a) 1971 San Fernando and (b) 1994 Northridge earthquakes.

4.4. *When does damage occur?*

The trends in Figure 10 suggest that changes of interval values of f_1 during strong shaking can be used as a simple *global* indicator of damage. A drop of f_1 (relative to its value for the initial time interval of weaker shaking) greater than a certain value (say about 20% for the Van Nuys building) would be an indicator that damage has occurred. Such an algorithm, implemented in a real-time structural health monitoring system, would have indicated that damage occurred in the Van Nuys building during the San Fernando and the Northridge earthquakes as early as about 10 s after trigger of strong motion recorders. We note here that such a rule applied to f_{sys} would not work, since it would have resulted in a false alarm during the Landers earthquake. Although Equation (4) suggests a constant relationship between f_{sys} and f_1 during linear and almost linear levels of response, that is not necessarily true for strong earthquake shaking, as indicated by this analysis.

Similarly, changes of the interval values of v_i can be used as *local* indicators of damage. For the Van Nuys building, the observed drops in v_i: (a) during the San Fernando earthquake of about 30% (from time interval S2 to S3) between the ground and 4th floor; and (b) during the Northridge earthquake of more than 20% (from time interval N1 to N2) between ground and 2nd floor, and 3rd and 6th floors, are all consistent with the locations of the observed damage. The large fluctuations of v_i between 2nd and 3rd floors for the WA, PA, MA, MO, SM L1, L2,

DOI: 10.1002/stc

and BB events appear to have been caused by the uncertainty in reading the impulse arrival times. Such large fluctuations can be eliminated or reduced significantly by fitting a model for the propagation times, which is beyond the scope of this work.

4.5. *Some force–displacement relationships inferred from wave travel times*

A general theory for *nonlinear* response of multi degree-of-freedom systems has yet to be developed. In the meantime, simplified representations, such as push over analysis, are used in seismic design. A typical push over analysis presents the base shear coefficient *versus* the displacement of the top of the structure, and describes a 'force–displacement relationship' of an 'equivalent' single degree of freedom system. In the following, we show how the results of our wave propagation analysis can also be viewed in such a form, for the purpose of comparison with previous results, and for understanding of how the two approaches compare.

Let $\bar{a}_{\max}$ be the average value of the peak interval acceleration, $\bar{a}_{\max} = (a_{\max}^{\mathrm{Gnd}} + a_{\max}^{\mathrm{Roof}})/2$ and let m be the mass of the building. Then $m\bar{a}_{\max}$ is a measure of the peak inertial force acting on the structure. The peak inertial force is approximately equal to the peak restoring force, which is proportional to $kd_{\max}$, where $d_{\max}$ is the peak *relative* displacement and k is the corresponding stiffness. Recalling that $\omega_{\mathrm{n}}^2 = k/m$, where ω_{n} is the circular natural frequency of an oscillator, we can expect that $\bar{a}_{\max} \approx d_{\max}\omega_1^2$ in both the linear and the nonlinear range of response for all time intervals considered in this analysis. Figure 13 shows $\bar{a}_{\max}$ *versus* $d_{\max}\omega_1^2$, where $\omega_1 2\pi f_1$ was computed using f_1 from the travel time analyses. It can be seen that all data points in this figure

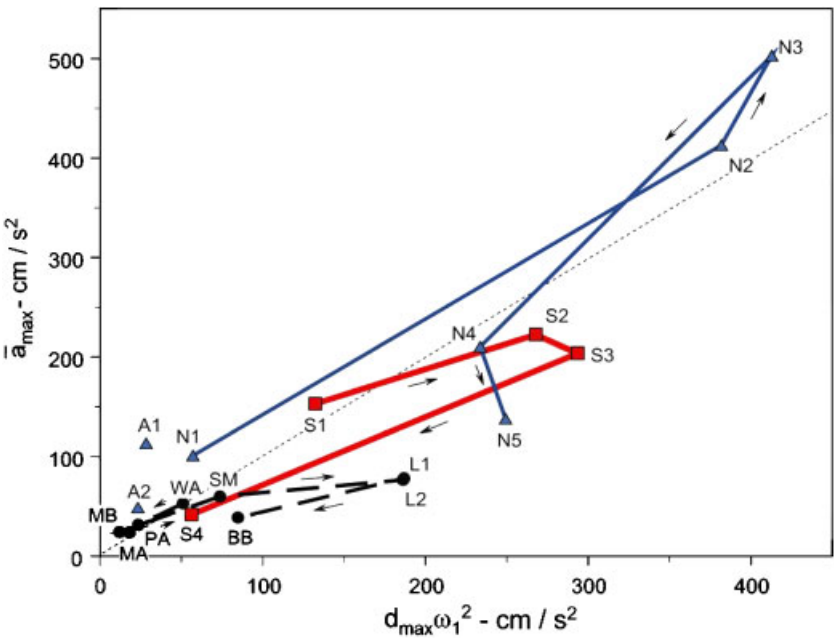

Figure 13. Average peak inertial force *versus* peak equivalent spring force (both per unit mass) during the 11 earthquakes. For the 1971 San Fernando and 1994 Northridge earthquakes, these values were computed, respectively, for four and five time segments (see Table II for identification of the time intervals).

DOI: 10.1002/stc

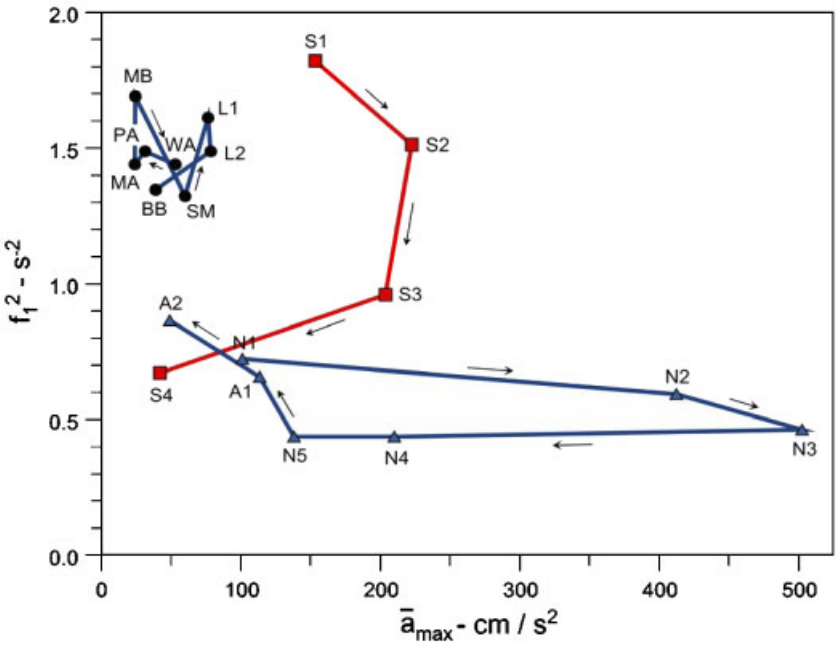

Figure 14. Normalized secant modulus *versus* average inertial force during the 11 earthquakes (see Table II for identification of the time intervals).

lie approximately along a 45° line, which confirms that f_1 estimated from wave travel times is physically meaningful. The departures from a straight line are at most about a factor of two, and include the influence of the soil–structure interaction (the effects of which on the peak relative response d_{max} could not be separated, due to inadequate instrumentation), the measurement errors in the estimates of f_1, and the occurrence of the peak ground and roof accelerations, and the peak roof displacements at different times.

Figure 14 shows f_1^2 *versus* $\bar{a}_{max}$, where the former is a measure of the secant modulus of the equivalent stiffness of the building ($\approx m\bar{a}_{max}/d_{max} \approx m\omega_n^2 d_{max}/d_{max} = m4\pi^2 f_1^2 \sim f_1^2$), and the latter is a measure of the force producing the deformation ($\approx m\bar{a}_{max} \sim \bar{a}_{max}$). It can be seen that the data points corresponding to the non-linear (damaging) responses during San Fernando and Northridge earthquakes are clearly separated from those corresponding to the essentially linear response during the WA, PA, MA, MO, SM, L1, L2, and BB events/intervals. The relatively small amplitude of f_1^2 for N1 (the first time interval of the Northridge earthquake) is probably due to the rapid growth of the strong motion amplitudes in this interval, but could also mean that the building was already 'softer' before the Northridge earthquake, because of the accumulated effects of all preceding earthquakes. Both clockwise loops S1–S2–S3–S4, and N1–N2–N3–N4–N5 are affected by the soil–structure interaction to a degree that cannot be quantified by this analysis.

Finally, Figure 15 shows $v_{base}/4f_1$ *versus* d_{max}, where the former is a measure of the average linear strain associated with a 1D shear wave transmitted into the building ($\sim v_{base}/\bar{\beta} = v_{base}/(4Hf_1)$, where v_{base} is the peak interval velocity at the ground floor, and $\bar{\beta} = 4Hf_1$ is the average shear wave velocity in the building), and the latter is a measure of the peak average drift

DOI: 10.1002/stc

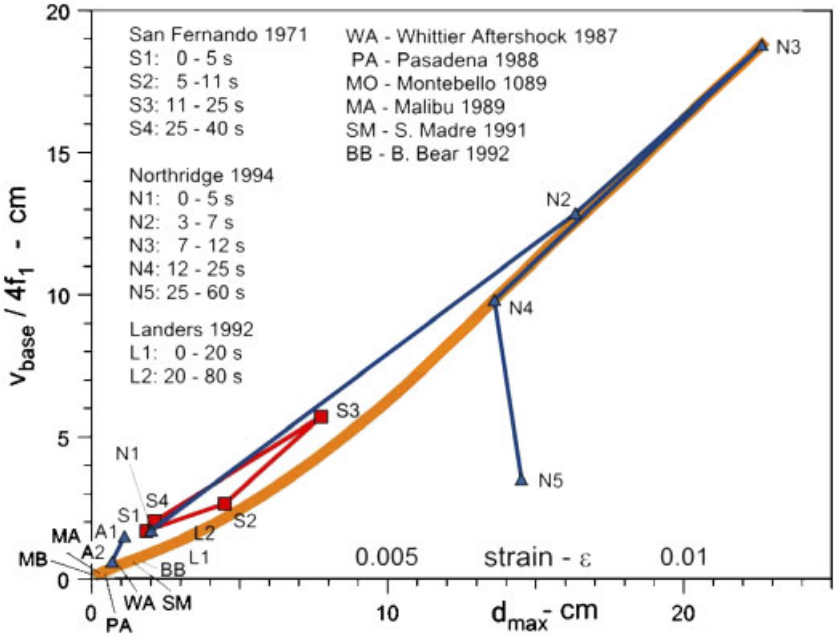

Figure 15. Peak linear shear strain *versus* peak average drift in the Van Nuys building during the 11 earthquakes.

in the building ($\approx d_{\max}/H$, where H is the building height). Therefore, we expect $v_{\text{base}}/4f_1 \sim d_{\max}$. Indeed, all the data points lie approximately along a straight line. For the Van Nuys building, $H = 20$ m and consequently $d_{\max} = 20$ cm corresponds to average strain of 1%. From the co-ordinates of the points in Figure 15 that correspond to the damaging events/time intervals, it can be seen that the damage began to occur for strains exceeding 0.002–0.003, as would be expected for a RC structure. The largest average strains for this group of 11 earthquakes occurred during the N3 segment of the Northridge earthquake.

5. DISCUSSION AND CONCLUSIONS

In this exploratory analysis of earthquake damage detection using wave travel times, as well as in our previous analysis of the Imperial County Services building [21], we applied the impulse response method in its most rudimentary form, based on several simplifying assumptions. One assumption is that 1D wave propagation up and down the structure can capture the principal features of the response, and that side reflections of the non-vertically propagating waves [40–42] can be neglected. Another assumption is that it is sufficient to work only with the recorded horizontal translations. Another group of assumptions is related to the transmission of the incident waves through the foundation. In particular, we assumed that we can neglect: (i) the effects associated with the horizontal propagation of seismic waves incident through the foundation [5, 43]; (ii) the structural response resulting from warping and deformation of the foundation [44]; and (iii) the rotational waves in the building caused by soil–structure

DOI: 10.1002/stc

interaction, and by the rotational components of the ground motion (associated with body P, and SV waves, and Rayleigh surface waves). Finally, we did not consider explicitly the detailed nature of the contributions of torsion and of rocking to the recorded horizontal EW translations.

The spatial resolution of the method depends on the number and the separation distance of the sensors, while its temporal resolution depends on the length of the time window chosen for the analysis. The wave travel times we measured by reading manually the impulse arrival times at different stations, with error of about $\Delta\tau \approx 0.01$ s. As it can be seen from Table II, the wave travel time over the height of the building changed during the San Fernando earthquake between $\tau_{tot} = 0.185$ and 0.305 s (or by $\Delta\tau_{tot} = 0.12$ s), and during the Northridge earthquake it changed between $\tau_{tot} = 0.295$ and 0.38 s (or by $\Delta\tau_{tot} = 0.085$ s). During the other smaller events, $\tau_{tot} \sim 0.2$ s. This implies that the error in reading the pulse arrival times, $\Delta\tau$, is about 20–30 times smaller than τ_{tot}, and about 10 time smaller than the change in travel time $\Delta\tau_{tot}$ interpreted to be due to damage. The determination of the wave travel times can be automated by fitting a model to the data.

The analysis of the Van Nuys building, presented in this paper, confirmed the findings of our previous study [21] that, despite the simplifying assumptions, even for time windows as short as about 5 s, the method yields physically meaningful impulse responses and wave travel times. The estimates of fixed-base frequency from the measured wave travel times were found to be consistent with the concurrent estimates of soil–structure system frequency. Finally, the changes in *fixed-base* frequency, f_1, and average floor velocities between sensors, v_i, we found to be consistent with the observed earthquake damage. In contrast, we found that tracking changes in the soil–structure system frequency can produce misleading inferences about the occurrence of damage, and can lead to false alarms.

Our analysis showed that, during the San Fernando earthquake, f_1 decreased by about 40% (relative to is value within the first 5 s from trigger), which corresponds to a decrease in the global rigidity of about 63% (see Table II). During the Northridge earthquake, f_1 decreased by about 22% (relative to is value within the first 3 s from trigger), which corresponds to a decrease in the global rigidity of about 40%. We also found that, although the first system frequency, f_{sys} was always smaller than f_1, their difference varied, contrary to what one could expect from a linear soil–structure interaction model (Equation (4)). The local changes of rigidity were as follows. During the San Fernando earthquake, the rigidity decreased by about 77% between the ground and 4th floors, and by about 48% between the 4th floor and roof. During the Northridge earthquake, the rigidity decreased by about 60% between ground and 2nd floors, by about 33% between 2nd and 3rd floors, and between 3rd and 6th floors, and by about 41% between the 6th floor and roof.

We conclude that analysis of wave travel times, *via* impulse response functions computed from the recorded seismic response, can provide useful and reliable information about the degree and spatial distribution of changes in stiffness of an instrumented building undergoing damaging response. Clearly, this method will be a useful tool for online structural health monitoring, and should be further improved and refined.

REFERENCES

1. Blume JA & Assoc. Holiday inn (Chapter 29). *San Fernando, California Earthquake of February 9, 1971*, vol. I, Part A. U.S. Department of Commerce, National Oceanic and Atmospheric Administration: Washington, DC, 1973.

DOI: 10.1002/stc

2. Mulhern MR, Maley RP. *Building Period Measurements Before, During and After the San Fernando, California, Earthquake of February 9, 1971*, vol. I, Part B. U.S. Department of Commerce, National Oceanic and Atmospheric Administration: Washington, DC, 1973; 725–733.
3. Islam MS. Analysis of the response of an instrumented 7-storey nonductile concrete frame building damaged during the Northridge earthquake. *Professional Paper 96-9*, Los Angeles Tall Building Structural Design Council, Annual Meeting, 1996.
4. Li YR, Jirsa JO. Nonlinear analyses of an instrumented structure damaged in the 1994 Northridge earthquake, *Earthquake Spectra* 1998; **14**(2):265–283.
5. Trifunac MD, Ivanović SS, Todorovska MI, Novikova EI, Gladkov AA. Experimental evidence for flexibility of a building foundation supported by concrete friction piles. *Soil Dynamics and Earthquake Engineering* 1999; **18**:169–187.
6. Trifunac MD, Ivanović SS, Todorovska MI. Seven storey reinforced concrete building in Van Nuys, California: strong motion data recorded between 7 February 1971 and 9 December 1994, and description of damage following Northridge 17 January 1994 earthquake. *Report CE 99-02*, Department of Civil Engineering, University of Southern California, Los Angeles, California, 1999.
7. Browning JA, Li RY, Lynn A, Moehle JP. Performance assessment for a reinforced concrete frame building. *Earthquake Spectra* 2000; **16**(3):541–555.
8. Ivanović S, Trifunac MD, Novikova EI, Gladkov AA, Todorovska MI. Instrumented 7-storey reinforced concrete building in Van Nuys, California: ambient vibration survey following the damage from the 1994 Northridge Earthquake. *Report No. CE 99-03*, Department of Civil Engineering, University of Southern California, Los Angeles, California, 1999.
9. Ivanović S, Trifunac MD, Novikova EI, Gladkov AA, Todorovska MI. Ambient vibration tests of a seven storey reinforced concrete building in Van Nuys, California, damaged by the 1994 Northridge Earthquake. *Soil Dynamics and Earthquake Engineering* 2000; **19**(6):391–411.
10. Ivanović S, Trifunac MD, Todorovska MI. On identification of damage in structures via wave travel times. *Proceedings of NATO Workshop on Strong Motion Instrumentation for Civil Engineering Structures*, Istanbul, Turkey, 2–5 June 1999. Kluwer: Dordrecht, 2001; 447–468.
11. De la Llera JC, Chopra AK, Almazan JL. Three-dimensional inelastic response of an RC building during the Northridge earthquake. *Journal of Structural Engineering* (ASCE) 2001; **127**(5):482–489.
12. Trifunac MD, Ivanović SS, Todorovska MI. Apparent periods of a building, part I: Fourier analysis. *Journal of Structural Engineering* (ASCE) 2001; **127**(5):517–526.
13. Trifunac MD, Ivanović SS, Todorovska MI. Apparent periods of a building, part II: time–frequency analysis. *Journal of Structural Engineering* (ASCE) 2001; **127**(5):527–537.
14. Todorovska MI, Ivanovic SS, Trifunac MD. Wave propagation in a seven-storey reinforced concrete building, part I: theoretical models. *Soil Dynamics and Earthquake Engineering* 2001; **21**(3):211–223.
15. Todorovska MI, Ivanovic SS, Trifunac MD. Wave propagation in a seven-storey reinforced concrete building, part II: observed wavenumbers. *Soil Dynamics and Earthquake Engineering* 2001; **21**(3):224–236.
16. Trifunac MD, Ivanović SS, Todorovska MI. Wave propagation in a seven-storey reinforced concrete building: III damage detection via changes in wave numbers. *Soil Dynamics and Earthquake Engineering* 2003; **23**(1):65–75.
17. Trifunac MD, Ivanović SS. Analysis of drifts in a seven-storey reinforced concrete structure. *Report CE 03-01*, Department of Civil Engineering, University of Southern California, Los Angeles, California, 2003.
18. Todorovska MI, Trifunac MD. Impulse response analysis of the Van Nuys 7-storey hotel during 11 earthquakes (1971–1994): one-dimensional wave propagation and inferences on global and local reduction of stiffness due to earthquake damage. *Report CE 06-01*, Department of Civil Engineering, University of Southern California, Los Angeles, CA, 2006.
19. Snieder R, Şafak E. Extracting the building response using interferometry: theory and applications to the Millikan Library in Pasadena, California. *Bulletin of Seismological Society of America* 2006; **96**(2):586–598.
20. Kohler MD, Heaton T, Bradford SC. Wave propagation in buildings. *Bulletin of the Seismological Society of America* 2007; **97**(4), in press.
21. Todorovska MI, Trifunac MD. Earthquake damage detection in the Imperial County Services Building III: analysis of wave travel times via impulse response functions. *Soil Dynamics and Earthquake Engineering* 2006, submitted.
22. Todorovska MI, Trifunac MD. Earthquake damage detection in the Imperial County Services Building I: the data and time–frequency analysis. *Soil Dynamics and Earthquake Engineering* 2007; **27**(6):564–576.
23. Todorovska MI, Trifunac MD. Earthquake damage detection in the Imperial County Services Building II: analysis of novelties via wavelets. *Soil Dynamics and Earthquake Engineering* 2006, submitted.
24. Doebling SW, Farrar CR, Prime MB, Shevitz DW. Damage identification and health monitoring of structural and mechanical systems from changes in their vibration characteristics: a literature review. *Report LA-13070-MS*, Los Alamos National Laboratory, Los Alamos, NM, 1996.
25. Chang PC, Flatau A, Liu SC. Review paper: health monitoring of civil infrastructure. *Structural Health Monitoring* 2003; **2**(3):257–267.

DOI: 10.1002/stc

26. Şafak E. Wave propagation formulation of seismic response of multi-storey buildings. *Journal of Structural Engineering* (ASCE) 1999; **125**(4):426–437.
27. Ma J, Pines DJ. Damage detection in a building structure model under seismic excitation using dereverberated wave machines. *Engineering Structures* 2003; **25**:385–396.
28. Trifunac MD. A three-dimensional dislocation model for the San Fernando, California, earthquake of February 9, 1971. *Bulletin of the Seismological Society of America* 1974; **64**:149–172.
29. Wald DJ, Heaton TH, Hudnut KW. The slip history of the 1994 Northridge, California, earthquake determined from strong motion, teleseismic, GPS and leveling data. *Bulletin of the Seismological Society of America* 1996; **86**(1B):S49–S70.
30. Trifunac MD, Hao TY. 7-storey reinforced concrete building in Van Nuys, California: photographs of the damage from the 1994 Northridge earthquake. *Report CE 01-05*, Department of Civil Engineering, University of Southern California, Los Angeles, California, 2001.
31. Trifunac MD, Brady AG, Hudson DE. Strong motion earthquake accelerograms, digitized and plotted data, Volume II, Part C. *Report EERL-72-51*, Earthquake Engineering Research Laboratory, California Institute of Technology, Pasadena, California, 1973.
32. Shakal A, Huang M, Darragh R, Cao T, Sherburne R, Malhotra P, Cramer C, Sydnor, Graizer V, Maldonado G, Petersen C, Wampole J. CSMIP strong-motion records from the Northridge, California Earthquake of January 17, 1994. *Report OSMS 94-07*, California Department of Conservation, Division of Mines and Geology, Office of Strong Motion Studies, 1994.
33. Lee VW, Trifunac MD. Automatic digitization and processing of accelerograms using PC. *Report 90-03*, Department of Civil Engineering, University of Southern California, Los Angeles, CA, 1990.
34. Kanai K. Some new problems of seismic vibrations of a structure. *Proceedings of the Third World Conference on Earthquake Engineering*, Auckland and Wellington, New Zealand, January 22–February 1, 1965; II-260–II-275.
35. Todorovska MI, Al Rjoub Y. Plain strain soil–structure interaction model for a building supported by a circular foundation embedded in a poroelastic half-space. *Soil Dynamics and Earthquake Engineering* 2006; **26**(6–7):694–707.
36. Todorovska MI, Al Rjoub Y. Effects of rainfall on soil–structure system frequency: examples based on poroelasticity and a comparison with full-scale measurements. *Soil Dynamics and Earthquake Engineering* 2006; **26**(6–7):708–717.
37. Todorovska MI. Estimation of instantaneous frequency of signals using the continuous wavelet transform. *Report CE 01-07*, Department of Civil Engineering, University of Southern California, Los Angeles, CA, 2001.
38. Celebi M, Phan LT, Marshal RD. Dynamic characteristics of five tall buildings during strong and low amplitude motions. *The Structural Design of Tall Buildings* 1993; **2**:1–15.
39. Dunand F, Gueguen Ph, Bard P-Y, Rodgers J, Celebi M. Comparison of the dynamic parameters extracted from weak, moderate and strong motion records in buildings. *Proceedings of the First European Conference on Earthquake Engineering and Seismology*, Geneva, Switzerland, 3–8 September 2006; Paper No. 1021.
40. Todorovska MI, Trifunac MD. Antiplane earthquake waves in long structures. *Journal of Engineering Mechanics* (ASCE) 1989; **115**(12):2687–2708.
41. Todorovska MI, Trifunac MD. A note on the propagation of earthquake waves in buildings with soft first floor. *Journal of Engineering Mechanics* (ASCE) 1990; **116**(4):892–900.
42. Todorovska MI, Lee VW. Seismic waves in buildings with shear walls or central core. *Journal of Engineering Mechanics* (ASCE) 1989; **115**(12):2669–2686.
43. Gičev V, Trifunac MD. Permanent deformations and strains in a shear building excited by a strong motion pulse. *Soil Dynamics and Earthquake Engineering* 2007. doi: 10.1016/j.soildyn.2007.01.001
44. Gičev V. Investigation of soil-flexible foundation—structure interaction for incident plane SH waves. *Ph.D. Dissertation*, Department of Civil Engineering, University of Southern California, Los Angeles, CA, 2005.

DOI: 10.1002/stc